Oligodendrocyte Dynamics in the Healthy Adult CNS: Evidence for Myelin Remodeling

Kaylene M. Young,[1,2,3] Konstantina Psachoulia,[1,6] Richa B. Tripathi,[1] Sara-Jane Dunn,[4] Lee Cossell,[2] David Attwell,[2] Koujiro Tohyama,[5] and William D. Richardson[1,*]

[1]Wolfson Institute for Biomedical Research and Department of Cell and Developmental Biology
[2]Department of Neuroscience, Physiology and Pharmacology
University College London, London WC1E 6BT, UK
[3]The Menzies Research Institute Tasmania, University of Tasmania, Hobart 7000, Australia
[4]Microsoft Research Cambridge, Cambridge CB3 0FB, UK
[5]The Center for Electron Microscopy and Bio-Imaging Research, Iwate Medical University, Morioka, Iwate 020-8505, Japan
[6]Present address: National Institutes of Health, NICHD, 35 Lincoln Drive, Bethesda, MD 20892, USA
*Correspondence: w.richardson@ucl.ac.uk
http://dx.doi.org/10.1016/j.neuron.2013.01.006

SUMMARY

Oligodendrocyte precursors (OPs) continue to proliferate and generate myelinating oligodendrocytes (OLs) well into adulthood. It is not known whether adult-born OLs ensheath previously unmyelinated axons or remodel existing myelin. We quantified OP division and OL production in different regions of the adult mouse CNS including the 4-month-old optic nerve, in which practically all axons are already myelinated. Even there, all OPs were dividing and generating new OLs and myelin at a rate higher than can be explained by first-time myelination of naked axons. We conclude that adult-born OLs in the optic nerve are engaged in myelin remodeling, either replacing OLs that die in service or intercalating among existing myelin sheaths. The latter would predict that average internode length should decrease with age. Consistent with that, we found that adult-born OLs elaborated much shorter but many more internodes than OLs generated during early postnatal life.

INTRODUCTION

The great majority of myelin-forming oligodendrocytes (OLs) are born in the early postnatal period (the first 4 weeks in mice) by differentiation of proliferative, migratory OL precursors (OPs). However, OPs continue to divide and generate new-myelinating OLs well into adulthood (Dimou et al., 2008; Rivers et al., 2008; Psachoulia et al., 2009; Kang et al., 2010; Zhu et al., 2011; reviewed by Richardson et al., 2011). The functional role of adult-born OLs is not known. Some brain regions such as the cortical gray matter and subcortical white matter contain a majority of unmyelinated axons even in 8-month-old mice, so it is conceivable that adult-born OLs simply myelinate the previously unmyelinated axons in those regions, perhaps changing

the functionality of that circuit and contributing in some way to neural plasticity (e.g., motor skills learning) (Fields, 2008; Richardson et al., 2011; Zatorre et al., 2012). An alternative possibility is that adult-born OLs are needed to preserve the normal complement of myelin in the face of OL turnover (death and replacement). However, there is no strong evidence for OL turnover during healthy young adulthood and indeed it is not clear whether myelinating OLs could die and be replaced without compromising myelin integrity, which is required for fast and efficient propagation of action potentials. This could be particularly problematic when one considers that most OLs maintain internodes on many different axons simultaneously (e.g., Butt et al., 1994).

Attempting to distinguish between the models outlined above—"de novo myelin genesis" versus "myelin remodeling"—was one of the aims of the work described here. We reasoned that, if adult-born OLs are mainly engaged in de novo myelination of previously naked axons, then one might expect to find very little new OL generation in a white matter tract like the adult optic nerve, which consists almost entirely of myelinated axons (Honjin et al., 1977; Bartsch et al., 1997; Dangata and Kaufman, 1997), compared with a tract like the corpus callosum, which contains a majority of unmyelinated axons (>70%) (Sturrock, 1980). On the other hand, if myelin remodeling is commonplace, then one might expect to find as much OL and myelin genesis in the optic nerve as in the corpus callosum.

In this study, we labeled OPs (which express platelet-derived growth factor receptor, alpha subunit [Pdgfra]) and their differentiated OL progeny in the postnatal and adult CNS by cumulative EdU (5′-ethynyl-2′-deoxyuridine) labeling and Cre-lox fate mapping in *Pdgfra-CreER[T2]* transgenic mice. This allowed us to estimate the rates of production of new OL lineage cells (both OPs and OLs) in different regions of the adult CNS. We determined that (1) all OPs, no matter where they reside, continue to divide at a slow rate into adulthood; (2) their rates of cell division depend on location (being slower in gray matter than in white matter and slower in optic nerve than corpus callosum, for example); (3) the rates of cell division in all regions decline with age, as previously reported; (4) substantial fractions
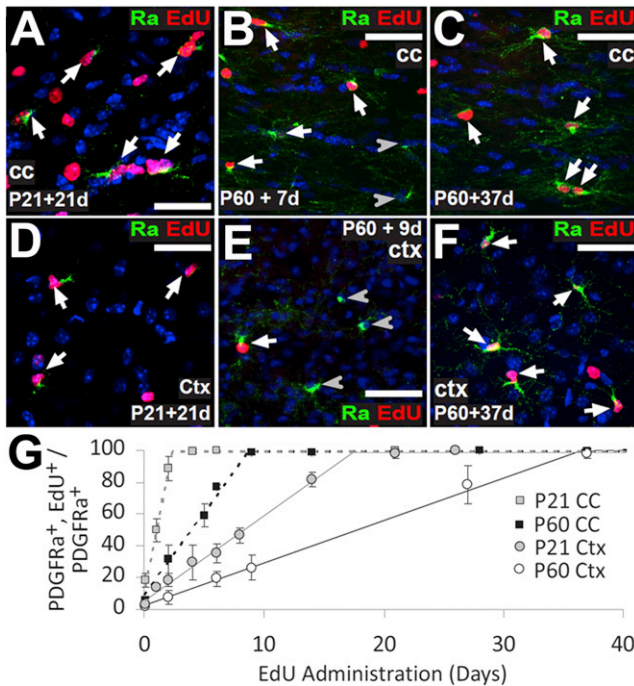
Figure 1. All OPs Proliferate in Forebrain Gray and White Matter at P21 and P60

(A–F) EdU was administered to P21 and P60 mice in the drinking water at 0.2 mg/ml, which we previously determined to be nontoxic (Figures S1 and S2). At various labeling times, coronal brain sections were processed to detect EdU (red) and immunolabeled for Pdgfra (green). Images are shown of the corpus callosum (cc) (P21, A; P60, B and C) and medial (primarily motor) cortex (ctx) (P21, D; P60, E and F).

(G) The labeling index was plotted against time of EdU administration (means ±SD, n = 3 mice). The maximum labeling index is the fraction of the OP population that is mitotically active (the growth fraction). In both cc and ctx, all OPs eventually incorporated EdU (GF = 100%). Arrows and arrowheads indicate Pdgfra$^+$, EdU$^+$ and Pdgfra$^+$, EdU-negative cells, respectively. Cell nuclei were stained with Hoechst 33258 (blue). Scale bars represent 25 μm.

Table 1. Cell-Cycle Parameters of Adult OPs in Different CNS Regions

P21		P60	
Corpus Callosum			
GF	99.8 ± 0.2	GF	99.2 ± 0.3
T	2.7 ± 0.2	T	9.5 ± 0.5
S	0.4 ± 0.1	S	0.8 ± 0.3
Cortex			
GF	97.8 ± 1.7	GF	98 ± 2.0
T	18.6 ± 1.4	T	36.3 ± 2.1
S	1.1 ± 0.4	S	1.0 ± 0.8
Spinal White Matter			
GF	98.1 ± 0.8	GF	99.2 ± 0.7
T	4.4 ± 0.3	T	14.9 ± 0.8
S	0.2 ± 0.4	S	1.1 ± 0.4
Spinal Grey Matter			
GF	98.1 ± 1	GF	98.8 ± 1.2
T	8 ± 0.7	T	27.4 ± 1.9
S	0.1 ± 0.3	S	0.8 ± 0.7
Optic Nerve			
GF	98.3 ± 0.7	GF	100 ± 0
T	7.6 ± 0.6	T	20 ± 1.7
S	0.6 ± 0.3	S	0.6 ± 0.4

A total of 0.2 mg/ml EdU was administered to P21 and P60 mice via their drinking water for up to 50 days. The proportion of Pdgfra$^+$ OPs that became EdU$^+$ was determined for various labeling periods (see Figures 1 and 2). From the cumulative labeling plots, we calculated the cell-cycle time (T, days), growth fraction (GF, %), and the duration of S phase (S, days) for OPs within the specified regions (Supplemental Experimental Procedures). Data are presented as mean ± SEM (n = 3 mice).

of the newly formed OLs survive and form myelin, even in the almost fully myelinated adult optic nerve; (5) adult-born OLs produce many more, shorter internodes than OLs that are born during early postnatal life. Our data are consistent with the idea that the rate of OP division is determined partly by the local density of unmyelinated axons, suggesting that one function of adult-born OLs might be to myelinate axons de novo in the adult. However, the number of new OLs and myelin internodes that accumulate in the adult optic nerve after postnatal day (P) 120 (>6% of all OLs) cannot be explained by de novo myelination of the small number of naked axons that persist in the nerve at that age (~1% of axons remain unmyelinated). Moreover, we found that the configuration of internodes (number and length) synthesized by a typical late-born OL is dramatically different from that of early-born OLs, although the total length of myelin synthesized by early- and late-born OLs is similar. We conclude that most of the new OLs produced in the adult optic nerve are engaged in myelin remodeling, either by replacing dying OLs in their entirety or by adding additional myelin internodes in such

a way that the total number of OLs increases without a concomitant increase in the total length of myelin sheath.

RESULTS

OP Cell-Cycle Duration Depends on Brain Region and Declines with Age

To detect cell division in vivo, we administered 5-ethynyl-2′-deoxyuridine (EdU; 0.2 mg/ml) to P21 and P60 mice via their drinking water for up to 50 days. Preliminary experiments had shown that this regimen was effective and nontoxic (Figures S1 and S2 available online). We visualized OPs by immunolabeling for Pdgfra and plotted the fraction of OPs that was EdU$^+$ (labeling index) versus time of EdU exposure (Figure 1). The cell-cycle time (T_C) was determined from this plot (Experimental Procedures; Table 1). In forebrain white matter (corpus callosum), T_C was ~3 days at P21 and ~10 days at P60 (Figure 1A–1C and 1G; Table 1). In the gray matter (motor cortex), T_C was longer (~19 days at P21 and ~36 days at P60) (Figure 1D–1G). The extended T_C in gray versus white matter is not due to a longer S phase (Table 1) and presumably reflects a longer time spent in early G1. These data support our previous conclusions that OPs in the white matter proliferate more rapidly
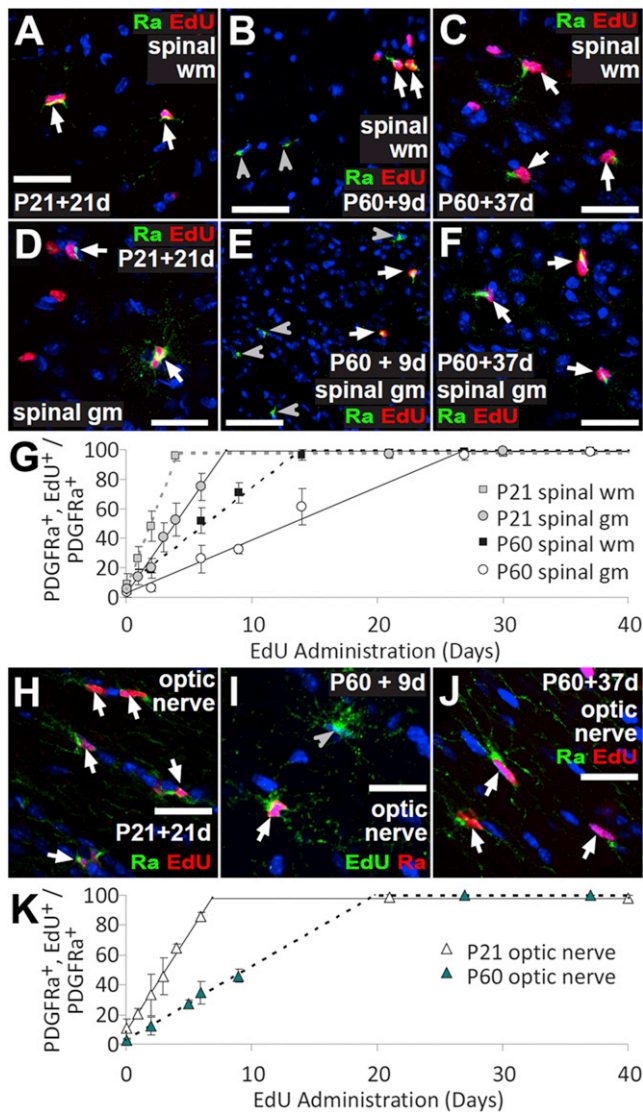
Figure 2. All OPs in the Spinal Cord and Optic Nerve Are Proliferating at P21 and P60

(A–F) Dividing OPs were labeled by continuous EdU administration to P21 and P60 mice via their drinking water at 0.2 mg/ml. Images are shown of spinal cord white matter (spinal wm) labeled with Pdgfra and EdU after EdU administration from P21 (A) or P60 (B and C) and of spinal cord gray matter (spinal gm) that was EdU labeled from P21 (D) or P60 (E and F).

(G–J) The percentages of Pdgfra+ OPs that were EdU labeled (labeling index) were plotted against EdU labeling time (G). Also shown are images of optic nerve labeled to detect Pdgfra and EdU following labeling from P21 (H) or P60 (I and J).

(K) The EdU labeling index in optic nerve was plotted against EdU labeling time (means ±SD, n = 3 mice). The maximum labeling index (GF) was 100%. Arrows and arrowheads indicate Pdgfra+, EdU+ and Pdgfra+, and EdU-negative cells, respectively. Cell nuclei were stained with Hoechst 33258 (blue). Scale bars represent 25 μm.

which suggested that around half of OPs are mitotically inactive (Psachoulia et al., 2009), cumulative labeling with EdU indicates that all OPs are cycling (growth fraction [*GF*] = 100%), both in gray and white matter.

We extended these observations to other parts of the CNS: the spinal cord gray and white matter (Figure 2A–2G) and the optic nerve, an exclusively white matter tract (Figure 2H–2K). At both P21 and P60, all OPs in these regions were mitotically active (Figure 2G and 2K). Furthermore, the cell cycle slowed down with age in each of these regions (Table 1). Cell-cycle time was not the same in all white matter regions; at P60, T_C was ~10 days in corpus callosum, ~15 days in spinal cord white matter, and ~20 days in optic nerve (Table 1). T_C was also longer in P60 cortical gray matter (~36 days) than in spinal cord gray matter (~27 days). Nevertheless, there was a general trend for OPs in gray matter to cycle more slowly than those in white matter (Table 1).

OPs Generate Differentiated OLs throughout the Adult CNS

We followed the fates of OPs in *Pdgfra-CreER^T2^: R26R-YFP* mice following tamoxifen administration at P60. At various times after tamoxifen, sections of brain (Figures 3A and 3B), spinal cord (Figures 3C and 3D), and optic nerve (Figure 3E) were immunolabeled for yellow florescent protein (YFP) and the adenomatous polyposis coli (APC) antigen, recognized by monoclonal antibody CC1, to detect newly differentiated OLs. Newly generated YFP+,CC1+ OLs were readily detected in all regions of the CNS, even at short times after the first dose of tamoxifen (e.g., after 7 days, P60+7), and they continued to accumulate until at least P60+320 (Figure 3F). As YFP+ cells acquired CC1 reactivity, they lost expression of Pdgfra. For example, at P60+42, 61% ± 3% of YFP+ cells in the spinal cord white matter were Pdgfra+ and 41% ± 3% were CC1+. In the spinal cord gray matter, 61% ± 5% were Pdgfra+ and 34% ± 6% were CC1+. Consistent with our previous experiments in which we examined OL genesis in the forebrain at P45 (Rivers et al., 2008) or P240 (Psachoulia et al., 2009), the rate of OL genesis in the motor cortex was significantly lower than in the corpus callosum. In fact, new YFP+, CC1+ OLs accumulated more rapidly in all white matter regions examined compared to the gray matter. Surprisingly, production of long-term-surviving OLs was similar in the highly myelinated optic nerve and the partially myelinated corpus callosum (Figure 3F); in both regions, ~65% of YFP+ cells were CC1+ at P60+320 (69% ± 4% and 64% ± 2% in corpus callosum and optic nerve, respectively). This implies that the probability of a given OP differentiating into an OL during a given time period is similar in both tracts. Because the number-density of OPs is fairly uniform throughout the CNS, including the optic nerve (Pringle et al., 1992), and because the cell-cycle time in optic nerve is about twice that in corpus callosum (Table 1), this means that over a set time about twice as many OLs are generated per unit volume in the corpus callosum than in the optic nerve.

Adult-Born OLs Have Classic, Myelinating Morphology
Although CC1 labeling demonstrates OL differentiation, it does not prove that those OLs form myelin sheaths. To identify newly
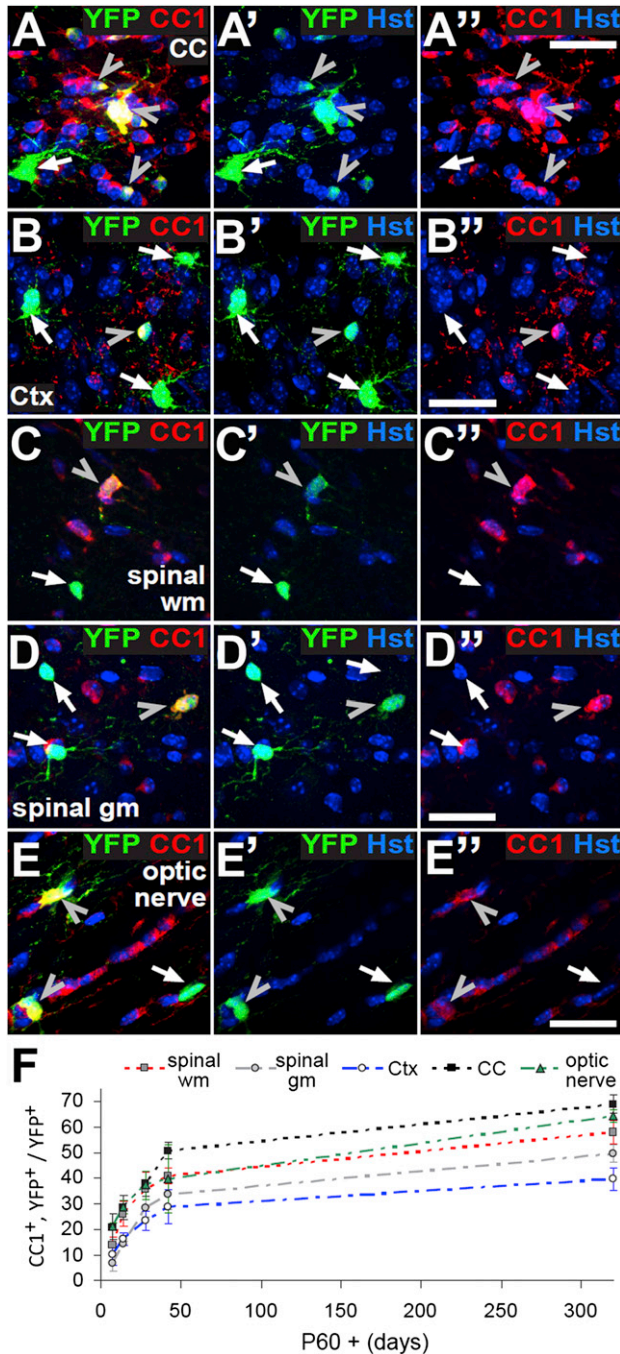
than in gray matter and that the rate of OP proliferation declines with age (Psachoulia et al., 2009). However, contrary to our previous bromodeoxyuridine (BrdU) labeling experiments,

Figure 3. OPs Generate Differentiated OLs throughout the Healthy Adult CNS

(A–E) Tamoxifen was administered to *Pdgfra-CreER^T2: R26R-YFP* transgenic mice at P60. Photomicrographs of the corpus callosum (cc) (A), motor cortex (ctx) (B), spinal cord white matter (spinal wm) (C), spinal cord gray matter (spinal gm) (D), and optic nerve (E) were collected following immunolabeling with CC1 (red) and anti-GFP (green).

(F) The percentage of YFP$^+$ cells that were differentiated OLs (YFP$^+$, CC1$^+$/total YFP$^+$) was plotted against time after tamoxifen (mean ±SD, n = 3 mice). White arrows indicate YFP$^+$, CC1-negative cells. Arrowheads indicate double-labeled cells. Cell nuclei were stained with Hoechst 33258 (Hst, blue). Scale bars represent 15 μm.

formed myelinating OLs by morphology (Butt et al., 1994; McIver et al., 2005), we crossed *Pdgfra-CreER^T2* with *Tau-mGFP* reporter mice (Hippenmeyer et al., 2005). *Tau-mGFP* is active in neurons and OLs but not in OPs or other neural cells (Richter-Landsberg and Gorath, 1999) and is superior to *Rosa-YFP* for revealing OL morphology, either because the *Tau* promoter is more active than Rosa or because membrane-inserted green fluorescent protein (mGFP) is better than cytoplasmic YFP at revealing slender OL cell processes including the external tongue process, although it is still excluded from compact myelin (see Figure 7).

We administered tamoxifen to P45 (Figure S3) and P60 *Pdgfra-CreER^T2: Tau-mGFP* mice (Figure 4). At P60+37, mGFP$^+$ cells in the corpus callosum had small, spherical cell bodies with numerous rod-like processes that ran parallel to each other in the direction of the axons (Figure 4B). In the motor cortex, the cell processes were less dense, less numerous, and more randomly oriented but myelin profiles were still evident (Figure 4A). This is the anticipated morphology of an OL in the cortex because axons in gray matter are not all aligned with one another as they are in white matter (Murtie et al., 2007; Vinet et al., 2010) and is consistent with the myelinating morphology previously reported for adult-born cortical OLs (Kang et al., 2010; Zhu et al., 2011). Like new OLs in the motor cortex, new OLs added to the adult spinal cord gray matter were highly branched cells, with processes extending in all directions (Figure 4D). OLs added to the spinal cord white matter (Figure 4E) and the optic nerve (Figures 4C and 4F) had many parallel mGFP$^+$ internodes like those in the corpus callosum. All mGFP$^+$ cells were Olig2$^+$, a few of which were NG2$^+$ (Stallcup and Beasley, 1987), indicating that they were all OL lineage cells (Figure S3). No mGFP$^+$ cells in the cortex or corpus callosum were NeuN$^+$, suggesting that *Pdgfra$^+$* OPs in these regions do not generate neurons (Figure S3).

New OLs Continue to Be Generated in the Almost Fully Myelinated Adult Optic Nerve

To determine whether OPs in the optic nerve continue to differentiate into new OLs in older animals, we administered tamoxifen to *Pdgfra-CreER^T2: R26R-YFP* mice on 4 consecutive days from P120. A short time later (P120+7), 19.9% ± 3.2% of all optic nerve OPs (defined by NG2 immunolabeling) were YFP labeled (mean ±SD, n = 3 mice), less than in the adult corpus callosum (∼45%; Rivers et al., 2008) or spinal cord (∼39%; Zawadzka et al., 2010; Tripathi et al., 2010). After 65 days (P120+65), the optic nerves were immunolabeled for YFP, Olig2, and APC/CC1 (Figures 5A and 5B) or for YFP and NG2 (Figure 5C). All YFP$^+$ cells were OL lineage (Olig2$^+$) and approximately one-third of YFP$^+$ cells were differentiated OLs (Olig2$^+$, CC1$^+$) (Figure 5D). Of all CC1$^+$ cells in the optic nerves of *Pdgfra-CreER^T2: R26R-YFP* mice at P120+65, 1.3% ± 0.3% were CC1$^+$, YFP$^+$ (mean ±SD, n = 3 mice; >5,000 CC1$^+$ cells examined). Because only ∼20% of OPs were YFP-labeled by tamoxifen induction, this implies that 6.5% ± 1.5% [(1.3 ± 0.3) × 100/20] of all CC1$^+$ cells in the P185 optic nerve are born after P120. As shown in the following section, the total length of myelin sheath that is synthesized by adult-born OLs is similar to that synthesized by early-born
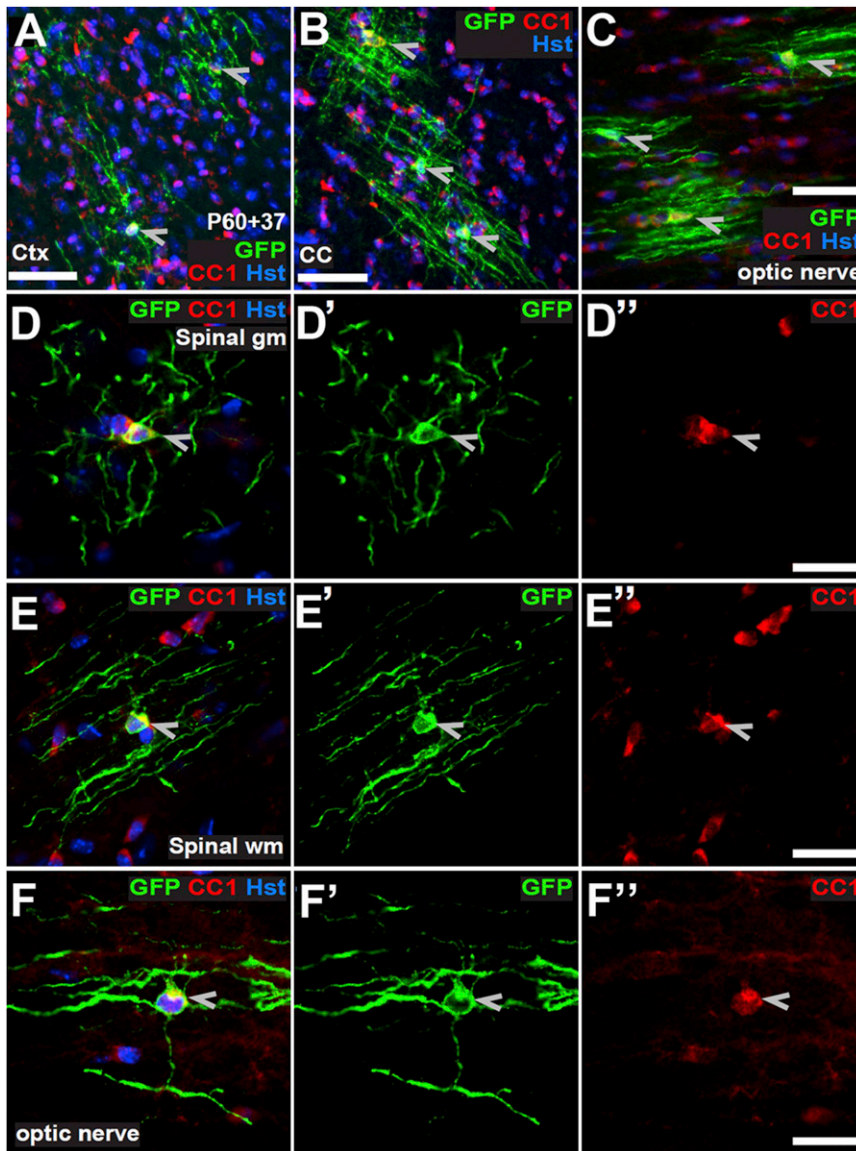
Figure 4. Adult-Born Myelinating OLs in Spinal Cord and Optic Nerve

(A–F) Sections of cerebral cortex and corpus callosum (A and B), spinal cord gray and white matter (D and E), and optic nerve (C and F) from P60+37 *Pdgfra-CreER^T2: Tau-mGFP* mice were immunolabeled with anti-GFP (green) and monoclonal CC1 (red). mGFP+, CC1+ myelinating OLs are shown (arrowheads). Shown are compressed z stacks (A–C) or single confocal scans (D–F). Cortex, *ctx*; corpus callosum, *cc*; gray matter, *gm*; white matter, *wm*; optic nerve. The corpus callosum and cerebral cortex of *Pdgfra-CreER^T2: Tau-mGFP* mice were also examined at P45+150 (Figure S3) Cell nuclei were counterstained with Hoechst 33258 (Hst, blue). Scale bars represent 25 μm (A–C) or 8 μm (D–F).

(mean ±SD, n = 18 OLs; range 11–35) of length 76 ± 2 μm (mean ±SEM, n = 271 internodes; range 12–234 μm), whereas OLs born between P120 and P185 possessed 77 ± 7 internodes per OL (mean ±SD, n = 15 OLs; range 41–125) of length 22 ± 1 μm (mean ±SEM, n = 702 internodes; range 6–293 μm). Therefore, compared to early-born OLs, the late-born OLs elaborate more than three times more internodes of less than one-third of the length (Figure 6E). Despite their short length, mGFP+ internodes formed after P120 frequently terminated at typical nodal structures that immunolabeled for the paranodal protein Caspr (Einheber et al., 1997) and clustered voltage-gated sodium channels (NaV1.6) (Figure 6H), indicating that they were functional myelin units. Of 144 mGFP+ internodes examined in one experiment, 136 (>94%) were clearly Caspr+ (Figures 6F and 6G), possibly an underestimate because some internodes might have terminated outside of the section. Tandem pairs of mGFP+ internodes were not observed, indicating that individual late-born OLs do not synthesize adjacent internodes along the same axon.

The fact that early-born OLs have longer internodes than those born later raises the question, "do early-born internodes shrink with time?" We addressed this question by administering tamoxifen to *Pdgfra-CreER^T2: Tau-mGFP* mice at P50 and analyzing OLs in their optic nerves at either P50+30 or P50+65. There were no significant differences in either the number of internodes per OL (21 ± 8 at P50+30, 27 ± 6 at P50+65; mean ±SD, n = 10 OLs at each age) or their average lengths (40 ± 3 μm at P50+30, 44 ± 4 μm at P50+65; means ±SEM, n > 140 internodes) (Figure 6). This demonstrates that internode lengths do not shrink appreciably between 30 and 65 days after tamoxifen. The mean length of internodes at both P50+30 (~40 μm) and P50+65 (~44 μm) fell between
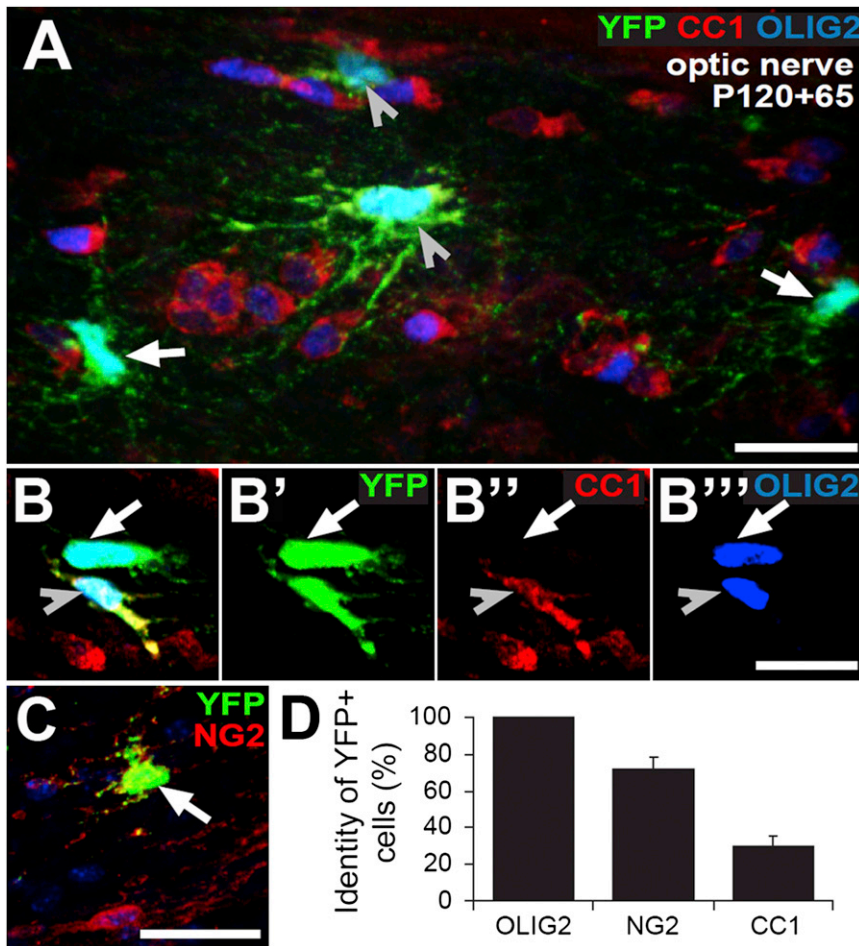
OLs, so there is a large disparity between the proportion of new myelin that is laid down in the optic nerve after P120 (~6.5% of the total) and the proportion of axons that remains unmyelinated at that time (~1%) (Honjin et al., 1977; Dangata et al., 1996).

Late-Born OLs Generate Many More, Shorter Internodes Than Early-Born OLs

We used the *Tau-mGFP* reporter strain to compare the morphology of OLs born between P30 and P60 (P30+30) to those born between P120 and P185 (P120+65) (Figure 6). In optic nerves of both P30+30 (Figure 6A) and P120+65 (Figures 6B and 6C) *Pdgfra-CreER^T2: Tau-mGFP* mice, individual mGFP+ OLs elaborated many internodes on different axons. However, early-born OLs produced fewer, longer internodes than their late-born counterparts (Figure 6D); individual OLs born between P30 and P60 possessed 21 ± 7 internodes

Figure 5. Differentiated OLs Are Generated in the Optic Nerve after Four Months of Age

(A and B) Sections of optic nerve from P120+65 *Pdgfra-CreER^T2: R26R-YFP* mice were immuno-labeled with anti-GFP (YFP+ cells; green), mono-clonal CC1 (OLs; red), and anti-Olig2 (all OL-lineage cells; blue). Shown are a confocal stack (A) and a single confocal scan (B).

(C) Adjacent sections were immunolabeled with anti-GFP (YFP+ cells; green) and anti-NG2 (OPs; red).

(D) The percentages of YFP+ cells that were OL lineage cells (YFP+, Olig2+), OPs (YFP+, NG2+), or differentiated OLs (YFP+, CC1+) were determined (means ±SD, n = 3 mice). Scale bars represent 15 μm.

the longer term, as observed here, has not previously been reported for the mouse optic nerve (Dangata et al., 1996). The age-dependent increase in fiber diameter that we detected was not accompanied by a significant change in g-ratio of bulk myelin between P30+30 (0.73 ± 0.06, n = 94) and P120+65 (0.74 ± 0.05, n = 83) (K-S test, p = 0.8; Figure 7E). However, there was a modest but significant increase in the g-ratio of newly formed (mGFP+) myelin, from 0.72 ± 0.05 (n = 86) in P30+30 nerves to 0.75 ± 0.06 (n = 79) in P120+65 nerves (p = 0.001; Figure 7F). These data indicate that late-born OLs generate internodes with a reduced ratio of myelin thickness to axon diameter compared to myelin that was formed earlier. The fact that we could not detect a statistically significant difference between the g-ratio for bulk myelin at P30+30 and for bulk myelin at P120+65 is presumably because the late-formed myelin with the slightly higher g-ratio is only a small fraction of the total.

those at P30+30 (~76 μm) and P120+65 (~22 μm), confirming that internode length is determined primarily by the age at which the myelin is laid down rather than by the time elapsed since its formation.

We identified newly formed myelin sheaths in the electron microscope, both by diaminobenzidine (DAB) immunohisto-chemistry and immunogold labeling, identifying recently formed internodes by their association with an mGFP+ external cyto-plasmic tongue process (Figures 7A–7D, 7G, and 7H). Myelin formed after P120 consisted of tight membrane wraps (Figures 7D and 7G) indistinguishable from the bulk of mGFP-negative myelin that had formed earlier. Recently formed OLs (mGFP+) visualized at P30+30 myelinated smaller diameter axons than recently formed OLs visualized at P120+65, having an average diameter of 421 ± 141 nm (mean ±SD, n = 86) compared with 524 ± 174 nm (mean ±SD, n = 79), respectively (p < 0.001, Kol-mogorov-Smirnov [K-S] test; Figure 7F). However, this probably reflects the overall increase in axon diameter detected in P120+65 versus P30+30 nerves (535 ± 195 nm, n = 83 versus 421 ± 139 nm, n = 94, respectively) (K-S test, p < 0.001; Figure 7E) rather than a change in the axonal targets of new OLs at different ages. Axon caliber increases following initial myelination, presumably as a result of myelination (Foster et al., 1982), but a further increase in the diameter of myelinated axons over

DISCUSSION

All NG2 Glia Continue to Divide during Adulthood

We previously reported, from cumulative BrdU labeling experiments (1 mg/ml in the drinking water), that the GF of OPs in both gray and white matter was ~50% at all ages (Rivers et al., 2008; Psachoulia et al., 2009). This implied that around half of OPs were mitotically inactive. Other groups made similar observations; for example, Guo et al. (2010) reported that only ~25% of NG2+ OPs in the cortical gray matter incorporated BrdU after 20 days exposure via the drinking water. However, others reported a higher growth fraction; Simon et al. (2011) reported that ~80% of neocortical gray matter OPs incorporated BrdU during a 37 day labeling period, and Kang et al. (2010) reported that all OPs incorporated BrdU during ~30 days. We now accept that our previous estimate of GF≈50% was too low, possibly reflecting suboptimal antigen retrieval or inhibition of
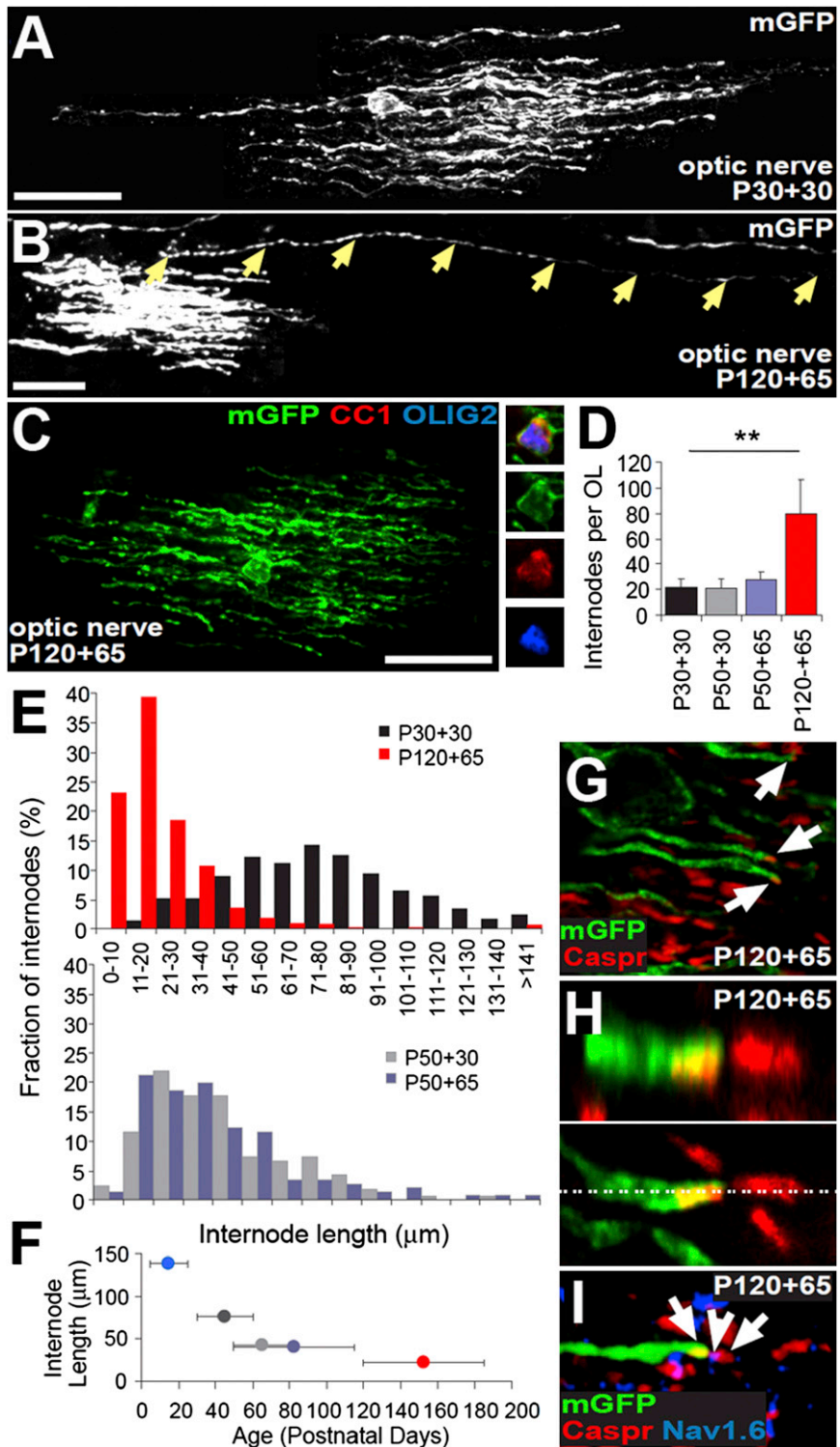
Figure 6. Late-Born OLs Make Many More, Shorter Internodes than Early-Born OLs

(A) Optic nerve sections from P30+30 *Pdgfra-CreER^T2^: Tau-mGFP* mice were immunolabeled with anti-GFP (white) (confocal stack).

(B) Optic nerve sections from P120+65 *Pdgfra-CreER^T2^: Tau-mGFP* optic nerves were immunolabeled with anti-GFP (white) (confocal stack). Arrows indicate a single long internode (293 μm in this example).

(C) Sections of P120+65 *Pdgfra-CreER^T2^: Tau-mGFP* optic nerves were immunolabeled with anti-GFP (green), anti-Olig2 (blue) and monoclonal CC1 (OLs; red) (confocal stack). A single confocal scan through the cell body is shown on the right.

(D) Quantification of the number of internodes per OL (means ±SD). The numbers are corrected for the sampling error introduced by the fact that only a fraction of the internodes of a given OL could be contained within the section; how the correction factor was derived is explained in Figure S4.

(E) Distributions of internode lengths for OLs born between P30 and P60 (black bars) or P120 and P185 (red bars) (n = 288 and n = 702 internodes, respectively) and between P50 and P80 (gray bars) or P50 and P115 (blue bars) (n = 164 and n = 146, respectively). The K-S test determined that internode lengths were not normally distributed but that the internode length distribution was significantly different for mGFP⁺ OLs in the P30+30 and P120+65 nerves (p < 10⁻⁶). The internode length distributions of mGFP⁺OLs in P50+30 and P50+65 nerves were indistinguishable (p = 0.1, K-S test).

(F) Average lengths of newly formed (mGFP⁺) internodes as a function of age of animal. There is a progressive reduction in internode lengths with age. The blue data point is taken from Butt et al. (1994), assuming that the internodes they measured had been generated at the peak of OL production around P10–P20 (Skoff et al., 1969).

(G) Sections of P120+65 *Pdgfra-CreER^T2^: Tau-mGFP* optic nerves were immunolabeled for mGFP (green) and the paranodal protein Caspr (red) (single confocal scan). mGFP⁺ myelin sheaths frequently terminated (136/144 times) at a Caspr⁺ paranode (white arrows).

(H) mGFP⁺ Caspr⁺ paranodes were always opposed by mGFP-negative, Caspr⁺ paranodes. X-Z compressed confocal stack (upper panel) and single X-Y confocal scan (bottom panel). (I) Sections from the same nerves were immunolabeled for mGFP (green), Caspr (red) and Nav1.6 (blue). White arrows indicate Caspr⁺ paranodes and white arrowhead indicates a Nav1.6⁺ node. Scale bars represent 30 μm (A–C).

cell division by BrdU (see Figure S2). Now, by cumulative labeling with EdU (which does not require antigen retrieval), we are able to label all OPs throughout the adult CNS (GF ≈ 100%), indicating that all OPs are capable of undergoing cell division (Clarke et al., 2012; this paper).

Age-Dependent Rate of Division

By underestimating *GF* 2-fold, we previously underestimated the cell-cycle time (T_C) of OPs by 2-fold at all ages (because $T_C = GF/m$ and *m* does not change; Figure S2; Supplemental Experimental Procedures). For example, we now recalculate
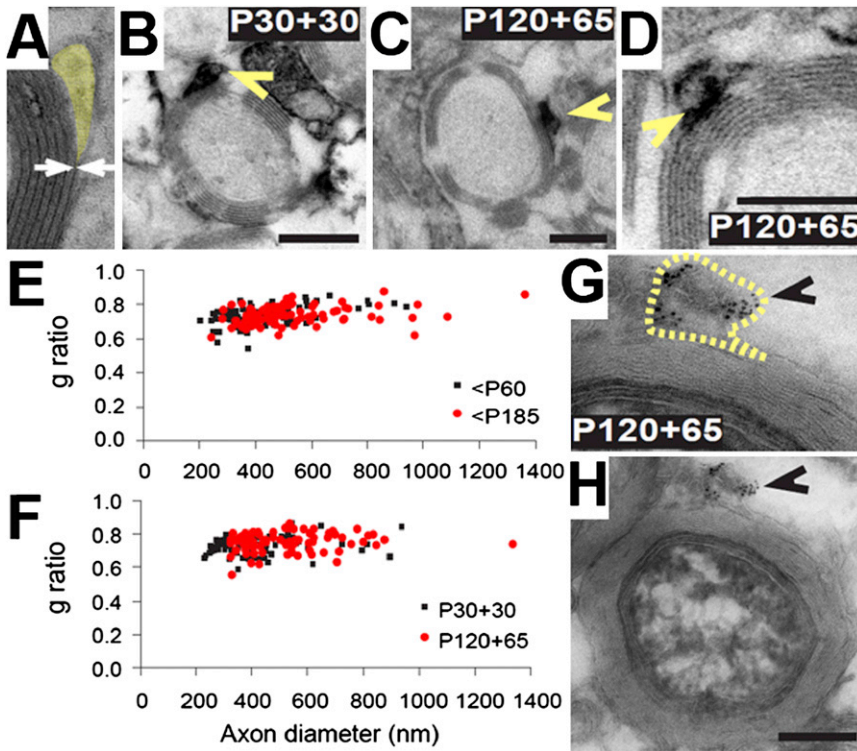
Figure 7. Adult-Born OLs Make Compact Myelin

(A) An illustrative electron micrograph of a myelinated axon in the P60 optic nerve. The external cytoplasmic tongue process has been pseudo-colored yellow.

(B) An electron micrograph of an axon that has been myelinated by an mGFP+ OL in a P30+30 *Pdgfra-CreER^T2: Tau-mGFP* optic nerve. The DAB reaction product identifies the mGFP+ cytoplasmic tongue of the corresponding myelin internode (indicated by an arrowhead).

(C) An electron micrograph of an axon that has been myelinated by an mGFP+ OL in a P120+65 *Pdgfra-CreER^T2: Tau-mGFP* optic nerve. The DAB+ cytoplasmic tongue is indicated (arrowhead).

(D) A higher-magnification image showing compact myelin synthesized by an mGFP+ OL in a P120+65 *Pdgfra-CreER^T2: Tau-mGFP* optic nerve.

(E) A scatterplot of axon diameter versus g-ratio for mGFP-negative myelinated axons in the P60 and P185 mouse optic nerves.

(F) The equivalent scatterplot for axons myelinated by recently formed (mGFP+) OLs in P30+30 and P120+65 *Pdgfra-CreER^T2: Tau-mGFP* nerves.

(G) Immunogold labeling of late-born mGFP+ OLs (born P120-P185) confirms that mGFP is restricted to the external tongue (outlined in yellow) and does not enter the myelin sheath. (H) Lower magnification of (G). Scale bars represent 200 nm.

T_C in the cortical gray matter of P60 mice to be ~36 days, in close agreement with a recent estimate of ~37 days in 2- to 3-month-old mice (Simon et al., 2011). We reported previously that T_C in the cortical gray matter increases linearly with age from early postnatal ages until at least P540 (Psachoulia et al., 2009). This remarkable conclusion still stands, although the rate of increase with time is greater than previously estimated: for every day after birth, T_C in the cortical gray matter increases by about two-thirds of a day, not one-third as previously estimated (Psachoulia et al., 2009). In the present study, we show that T_C increases with age not only in the cortical gray and white matter but also in the spinal cord gray and white matter and in the optic nerve (Table 1). Our data are in keeping with a recent study that reported age-dependent slowing of the OP cell cycle in the mouse spinal cord (Lasiene et al., 2009).

Control of OP Proliferation by Axons?

Age is not the only factor that influences the proliferative rate of OPs. In the P60 spinal cord, for example, OPs in the gray matter divided more slowly ($T_C \approx 27$ days) than in the white matter ($T_C \approx 15$ days). In the P60 optic nerve (an exclusively white matter tract), OPs proliferated more slowly ($T_C \approx 20$ days) than in either spinal cord white matter ($T_C \approx 15$ days) or corpus callosum ($T_C \approx 10$ days) (Table 1). Moreover, OPs in either the cortical or spinal cord gray matter were dividing more slowly ($T_C \approx 36$ or 27 days, respectively) than in any of the white matter regions examined. These data suggest that the local environment strongly affects the proliferation rate of OPs. The fact that there are many more unmyelinated axons in the adult corpus callosum ($T_C \approx 10$ days) than in the optic nerve ($T_C \approx 20$ days)

suggests that the local density of unmyelinated axons might be one factor that influences local proliferation rates, perhaps because mitogens are released from or associated with the surfaces of unmyelinated axons. Against this idea, we showed previously that an important neuron-derived OP mitogen, platelet-derived growth factor (A-chain homodimers, Pdgf-AA), is released from neuronal cell bodies in the retina but not from their axons in the optic nerve (Fruttiger et al., 2000). It is possible that naked axons exert an indirect mitogenic effect in white matter; for example, through activity-driven release of Pdgf or other mitogens from local astrocytes, as suggested by Barres and Raff (1993). Cell-intrinsic differences in the proliferative properties of OPs from different CNS regions have also been reported (Power et al., 2002).

A Significant Fraction of Adult-Born OLs Survive Long-Term

It has been estimated that ~50% of OLs in the perinatal optic nerve die soon after they are formed (Barres et al., 1992). In the developing neocortex, ~20% of premyelinating OLs die between P7 and P11 (Trapp et al., 1997). Because the number-density of OPs within a given region does not change much with age (Rivers et al., 2008), it follows that half of the daughters of OP divisions must either differentiate (and lose OP markers) or die. Therefore, by comparing our measured rates of OP proliferation and OL production, we can deduce the amount of cell death. For example, in the P60 corpus callosum, the OP cell-cycle time (T_C) is ~9.5 days (Table 1), implying that a number of new cells equal to the starting population must be formed within 9.5 days (because all OPs are dividing). If all of these

additional cells were to differentiate into OLs and survive, and assuming that the cell-cycle time continues to increase linearly with age after P60 at the same rate that it increases between P21 and P60 (Table 1), then we can calculate that 77% of all YFP$^+$ cells in the corpus callosum of P60+42 *Pdgfra-CreER^{T2}: R26R-YFP* mice should be CC1$^+$ OLs (see Supplemental Experimental Procedures). In fact, we found by experiment that ∼50% of YFP$^+$ cells were CC1$^+$ OLs (Figure 3F), so ∼30% of adult-born OLs survive at least 42 days in the corpus callosum (Supplemental Experimental Procedures). For P60 optic nerve (T_C ≈ 20 days), we calculate that in the absence of cell death ∼62% of YFP$^+$ cells should be CC1$^+$ OLs within 42 days, whereas we found only ∼40% (Figure 3F), implying that ∼41% of OLs survive long-term. There is considerable uncertainty in these calculations concerning the rate of increase of T_C with age; they possibly underestimate the proportion of new OLs that survives because the cell cycle probably slows down (T_C increases) more rapidly after P60 than is assumed here (Psachoulia et al., 2009). Nevertheless, the data suggest that a significant fraction of adult-born OLs survive long-term, in keeping with previous reports that OLs continue to accumulate with age in the mouse corpus callosum (McCarthy and Leblond, 1988) and the primate optic nerve (Sandell and Peters, 2002; Peters, 2009).

Adult Myelin Genesis: Evidence for Myelin Remodeling

The scale of new OL genesis in the adult is unexpectedly large: ∼30% of all OLs present in the corpus callosum of 8-month-old mice are generated after 7 weeks of age (Rivers et al., 2008; Zhu et al., 2011). What is the function of the adult-born myelinating OLs? One possibility is that naked axons continue to be myelinated de novo throughout adult life. Many axons in the corpus callosum remain unmyelinated after development and some of these might become targets for myelination during adulthood. This would substantially alter the transmission properties of the axons involved and might, for example, facilitate motor skills learning or some other form(s) of neural plasticity (reviewed by Fields, 2008; Richardson et al., 2011; Zatorre et al., 2012). Alternatively, adult OL genesis might be required to maintain existing myelin sheaths, either through direct replacement of OLs that die in use or by more subtle remodeling of myelin sheaths in the absence of cell death. If so, this remodeling might be crucial to maintain or modify nervous system function throughout life. These two possibilities, de novo myelination and myelin remodeling, are not mutually exclusive.

In the rat optic nerve, the peak time of OL generation is ∼P10–P20 and ∼85% of axons are myelinated by P28 (Skoff et al., 1969). Myelination in the mouse optic nerve follows a similar course (Bartsch et al., 1997; Dangata et al., 1996; Dangata and Kaufman, 1997). It has been estimated that 98.8% of optic nerve axons are myelinated in 6- to 8-month-old mice (Honjin et al., 1977). Reinforcing this, a study of C57BL × CBA mice (F1 generation), similar to the genetic background of our mice, found that "practically all" optic nerve axons were myelinated by P112 (Dangata et al., 1996; Dangata and Kaufman, 1997). Therefore, if the main function of adult-born OLs is to myelinate previously unmyelinated axons, then we should not expect

much OL genesis in the optic nerve after P112 because there should be almost no naked axons available to myelinate. However, our observations contradicted this prediction; we found that ∼6.5% of CC1$^+$-differentiated OLs in the optic nerve were generated between P120 and P185, so there are many more adult-born OLs than would be required to myelinate the ∼1% of axons that remain unmyelinated at that age, given that late-generated OLs synthesize as much or more myelin sheath as those born earlier (see next paragraph). We conclude that the majority of optic nerve OLs born after P120 are unlikely to myelinate previously unmyelinated axons.

OLs born between P30 and P60 made ∼21 internodes of length ∼76 μm, whereas OLs born after P120 elaborated ∼77 internodes per cell of mean length ∼22 μm. OLs born between P50 and P80 made ∼21 internodes ∼40 μm in length, intermediate between earlier and later ages. Butt et al. (1994) measured randomly selected, dye-injected OLs in optic nerves from mice aged between P30 and P60, and counted ∼19 internodes per cell with an average length ∼138 μm. Because Butt et al. (1994) were not selecting recently formed OLs, most labeled OLs in their experiments would have been born in the early developmental period before P10–P20 (Skoff et al., 1969). Thus, late-forming OLs have many more internodes, much shorter in length, than early-born OLs. However, the total lengths of myelin sheath synthesized by early- and late-born OLs were similar; ∼1,600 μm per cell (21 × 76 μm) at P30–P60 compared to ∼1,700 μm per cell (77 × 22 μm) at P120–P185.

How do the internodes that we observed at P120+65 come to be shorter than those observed at P30+30? Were they synthesized short from the outset and remained that way, or were they synthesized long like early-born internodes but subsequently shrank? If the latter, then a longer waiting time after tamoxifen (65 versus 30 days) could have accounted for the observed difference in internode lengths. To address this possibility, we compared OLs in P50+30 versus P50+65 optic nerves. There were no significant differences in either the number of internodes per OL or the mean length of internodes, suggesting that those aspects of mature OL morphology are stable over at least 2 months. Therefore, from the information now available, it seems very likely that the chief determinant of internode number/length is the age at which the myelinating OL in question was generated, not the length of time it has been in existence. Our data and those of Butt et al. (1994) show that there is a progressive decrease in the lengths of newly formed internodes with advancing OL birthdate, from ∼140 μm in the early postnatal period (∼P10–P20), to ∼80 μm after P30, to ∼40 μm after P50, to ∼20 μm after P120 (Figure 6F). Our data are consistent with the observations that abnormally short myelin internodes accumulate with age in mouse spinal cord white matter (Lasiene et al., 2009) and that paranode frequency increases with age in the rhesus monkey brain (reviewed by Peters and Kemper, 2012). Despite most late-forming internodes being short, there were a few very long (>200 μm) stretches of new myelin sheath in P120+65 optic nerves (e.g., Figure 6B). These rare, longer internodes might represent de novo myelination of some of the small number of unmyelinated axons that remain in the P120 nerve. If so, one might expect to find more long stretches of newly formed myelin in the corpus callosum, which

contains many more unmyelinated axons (>70% remain unmyelinated in 8-month-old mice; Sturrock, 1980).

Our data suggest that the majority of adult-born internodes in the optic nerve are not engaged in de novo myelination but instead must replace or remodel pre-existing myelin. One possibility is that there is continuous death and replacement of OLs, each dying OL being replaced in its entirety by one or more new OLs. In this scenario, the fact that late-formed internodes are shorter than their early-formed counterparts would imply that each "old" internode of a putative dying OL is replaced by two or more "new" internodes. Despite examining hundreds of mGFP⁺ internodes of individual widely spaced OLs, we have never observed two new mGFP⁺ internodes side by side on the same axon. Therefore, we are confident that a given OL rarely, if ever, synthesizes two internodes side by side on the same axon; if new internodes are laid down in pairs, then each one of the pair must come from a separate OL. We estimated that ~4% of OPs in *Pdgfra-CreER^T2: Tau-mGFP* optic nerves recombined and became mGFP⁺ (Experimental Procedures), so ~4% of newly formed OLs should also be mGFP⁺ (because on average one new OL and one replacement OP is formed for every OP division) and ~4% of newly formed OLs that survive long-term will be mGFP⁺ (assuming that mGFP⁺ and GFP-negative OLs are equally likely to survive). Therefore, if new internodes always occurred in pairs, then we would have expected ~4% of mGFP⁺ internodes to have an mGFP⁺ neighbor. Since in one experiment we counted 144 (GFP⁺, Caspr⁺) paranodes, none of which flanked the same node, it is unlikely (p < 0.017, Poisson probability for zero or one occurrence when six are expected) that new, short mGFP⁺ internodes are usually assembled next to one another in the space vacated by a previous, longer internode. Our observations might more easily be explained by postulating that a dying internode can be replaced by a single new, short internode together with an expansion of one or both flanking internodes. However, it must be emphasized that we do not yet know whether there is significant turnover of OLs or myelin during the first year of life in mice. If not, it would imply that myelin can be remodeled in the absence of OL death. For example, OLs might shed internodes over time, the lost internodes being replaced piecemeal with internodes from newly formed OLs as described above. Alternatively, new myelin internodes might intercalate among existing internodes. It is known that adult OPs contact axons at nodes of Ranvier (Butt et al., 1999); perhaps this is in readiness for initiating new myelin sheath formation from the nodes, replacing the existing sheaths in one or both directions without exposing the axon.

Myelin that was synthesized after P120 had a significantly larger g-ratio (thinner myelin sheath relative to axon diameter) than myelin synthesized at earlier times (after P30). It is well documented that myelin formed during repair of experimental demyelination or during demyelinating injury or disease is thinner on average (larger g-ratio) than myelin that is formed during normal development (e.g., Lasiene et al., 2008), although this is less pronounced for smaller-diameter axons such as those in the optic nerve (Stidworthy et al., 2003). Remyelinating OLs also possess shorter internodes than developmentally generated OLs (Blakemore and Murray, 1981). Our data suggest that the thinner myelin and shorter internodes associated with remye-

lination might be a special example of adult myelination rather than a property of regenerated myelin per se.

What are the molecular mechanisms that determine internode length? Internode length and the number of internodes elaborated per OL vary greatly between CNS regions (Butt et al., 1994; Murtie et al., 2007; Chong et al., 2012) and are in part determined by the properties of the axons being myelinated (Almeida et al., 2011). The signaling mechanisms involved are largely unknown, although competition among OLs, partly mediated by Nogo-A, has been proposed as a potential mechanism (Chong et al., 2012). Recently, it has been shown that the social conditions experienced by mice can influence the morphological complexity of their OLs (including the number of internodes per OL) and that this is mediated by Neuregulin signaling through ErbB3 receptors on OLs (Makinodan et al., 2012). Ultimately, the biochemical pathways that control OL maturation, myelination, and morphology might be stimulated by electrical activity in axons (Wake et al., 2011).

How would axonal conduction speed be affected by the shorter internode length of later born OLs? Although internode length is not the only factor determining conduction speed, there are several reasons why it might be advantageous to the animal to adjust conduction speed with age. For example, it might be important to maintain a constant total transit time from retina to brain as the animal grows in size, or to synchronize arrival times of signals from different parts of the retina (Stanford, 1987). Such considerations may be important for motion detection in the visual system (Raz et al., 2012) and for other time-sensitive processes throughout the CNS (Kimura and Itami, 2009). To investigate the effect of a shorter internode length, we carried out simulations based on the models of Richardson et al. (2011) (see Supplemental Experimental Procedures). We found that the effect of internode length on conduction speed is strongly affected by how tightly the myelin is attached to the axon. With no periaxonal space between the axon and the myelin (and using an axon diameter of 0.524 μm and a node length of 0.8 μm), decreasing the length of all the internodes from 138 μm to 22 μm *increased* the conduction speed by 28% (from 1.83 to 2.34 m/s). This is as a result of excitation being conveyed more effectively from one node to another. However, with a 3 nm space between the axon and the myelin, switching to the shorter internode length produced a 7.5% *decrease* of conduction speed (from 1.02 to 0.94 m/s) as a result of a larger fraction of the axon length having its effective capacitance increased by short-circuiting of the myelin. Consistent with this, simulations published by Lasiene et al. (2009), assuming the existence of a periaxonal space, predicted that shorter internodes should decrease conduction speed. Since only a proportion of internodes will be shorter in the older animals, the magnitude of the speed changes in vivo will be smaller than those stated above, either with or without a periaxonal space.

EXPERIMENTAL PROCEDURES

Transgenic Mice and Cre Recombination

Homozygous *Pdgfra-CreER^T2* BAC transgenic mice (Rivers et al., 2008) were crossed with Cre-sensitive reporter mice—either homozygous *Rosa26R-YFP* (*R26R-YFP*) reporters (Srinivas et al., 2001) or heterozygous *Tau-lox-STOP-lox-mGFP-IRES-NLS-LacZ-pA* (*Tau-mGFP*) mice (Hippenmeyer et al.,

2005)—to generate double heterozygous offspring for analysis. Genotyping for Cre and *R26R-YFP* was by PCR amplification of genomic DNA as previously described (Rivers et al., 2008). PCR genotyping for *mGFP* (encoding a membrane-tethered version of GFP) was carried out using GFP-specific primers (5′-CCCTGAAGTTCATCTGCACCAC-3′ and 5′-TTCTCGTTGGGG TCTTTGCTC-3′). Tamoxifen (Sigma) was dissolved at 40 mg/ml in corn oil by sonicating at 21°C for 1 hr and administered to postnatal mice by oral gavage on four consecutive days (each dose was 300 mg tamoxifen/kg body weight). All animal experiments were approved by the Home Office of the UK Government under the Animals (Scientific Procedures) Act, 1986.

Tissue Preparation and Immunolabeling

Mice were perfusion-fixed with 4% (w/v) paraformaldehyde (PFA; Sigma) in PBS. Brain, spinal cord and optic nerve tissue was dissected and lightly post-fixed in 4% PFA at 21°C for either 45 min (coronal brain slice [∼0 to +2 mm Bregma] or ∼1 cm segment of spinal cord spanning the lower cervical and upper thoracic region) or 20 min (∼7 mm segment of the optic nerve at the retinal end). Optic nerves from some P30 and P120 mice, and brains from P45 mice, were postfixed in 4% PFA overnight at 4°C, where stated in the text. Tissue was cryoprotected in 20% (w/v) sucrose (Sigma) in PBS before freezing in OCT on the surface of dry ice. Next, 30 μm cryosections of the brain (coronal), spinal cord (transverse and longitudinal), and optic nerve (longitudinal) were collected and processed as floating sections (Young et al., 2007). Primary and secondary antibodies (see Supplemental Experimental Procedures for details) were diluted in PBS blocking solution (0.1% [v/v] Triton X-100 and 10% fetal calf serum in PBS) and applied to sections overnight at 4°C. Tris-buffered saline (TBS) was substituted for PBS when immunolabeling with anti-CC1 (Supplemental Experimental Procedures).

EdU Labeling and Detection

For cumulative labeling experiments, EdU (Invitrogen) was dissolved in the drinking water at 0.2 mg/ml, which we had determined to be nontoxic (Figures S1 and S2). The water was exchanged every 48 hr and mice were exposed to EdU for up to 50 days. Alternatively, EdU was dissolved in PBS at 5 mg/ml, filter sterilized, and administered as a single intraperitoneal injection of 25 mg EdU per kilogram body weight (Chehrehasa et al., 2009). EdU was visualized using the AlexaFluor-647 Click-iT EdU Cell Proliferation Assay Kit (Invitrogen) immediately after immunohistochemistry. Floating sections were incubated at 20°C–23°C for 15 min in PBS/0.5% (v/v) Triton X-100 and then transferred to the EdU developing cocktail, incubated in the dark at 20°C–23°C for 40 min, and washed in PBS. Cell nuclei were visualized by poststaining with Hoechst dye 33258 (1:1000, Sigma) and sections mounted under coverslips in fluorescence mounting medium (Dako Cytomation).

Microscopy and Cell Counts

Confocal images were collected using an UltraView confocal microscope (Perkin Elmer) with Volocity Software (Perkin Elmer) as z stacks with 1 μm spacing, using standard excitation and emission filters for DAPI, FITC (Alexa Fluor-488), TRITC (Alexa Fluor-568) and Far Red (Alexa Fluor-647). For quantifying cell numbers, low-magnification photomicrographs (×20 objective) of nonoverlapping fields were taken of the corpus callosum (∼8 fields/coronal section, between the dorsolateral corners of the lateral ventricles), medial (motor) cortex (12 fields/ section), optic nerve (∼8 fields/ longitudinal section), and spinal cord (∼20 fields/ transverse section). Cells were counted manually, viewing the photomicrographs using Adobe Photoshop software. Statistical comparisons were made using a t test or ANOVA, as specified. For quantifying internode number and length, confocal images were collected (×40 objective) through individual OLs with a visible cell body in longitudinal sections of isolated optic nerves. Transverse (end-on) views of OLs showed that their internodes were distributed more or less uniformly within a cylindrical field centered on the cell soma. Because section thickness ($T = 30$ μm) is less than the diameter of this cylinder ($d = 2r = 42 \pm 15$ μm, n = 18 at P30+30; 47 ± 12 μm, n = 10 at P50+30/65; 55 ± 15 μm, n = 15 at P120+65) (means ±SD), it introduces a sampling error (i.e., not all internodes of a given OL are within the section). We calculated the required correction (for $r < T < 2r$) to be $3\pi T/(3\pi T-4r) \approx 1.42$ for P30+30, 1.50 for P50+30/65, and 1.64 for P120+65 (Figure S4).

Comparison of internode length distributions was by the K-S nonparametric test (http://www.physics.csbsju.edu/stats/KS-test.n.plot_form.html).

Immunoelectron Microscopy

Following perfusion fixation, optic nerves were removed and immersed in 4% (w/v) PFA in PBS for 4 hr or overnight at 4°C. Tissue was stored in PBS at 4°C until being processed for electron microscopy (EM). Transverse 50 μm vibratome sections were rinsed in TBS (0.1M, pH7.6) and incubated in TBS containing 10% (v/v) normal goat serum at 20°C–23°C for 2 hr. The sections were then incubated with rabbit anti-GFP (1:100, Synaptic Systems) for 48 hr at 4°C, washed in TBS and incubated with horseradish peroxidase (HRP)-conjugated goat anti-rabbit IgG (1:100, Dako Cytomation) in TBS, for 24 hr at 4°C. Sections were washed in TBS and further fixed in 1% (v/v) glutaraldehyde. The signal was developed by incubating sections in TBS containing 0.01% (v/v) 3,3′-DAB and 0.01% (v/v) hydrogen peroxide at 20°C–23°C. Sections were then osmicated (0.5% [w/v] OsO_4) for 2 min), dehydrated in a graded series of ethanols, passed through QY1 (n-butyl glycidyl ether; Nisshin EM, Japan) and embedded in EPON resin (TAAB, UK). Ultrathin sections were examined in the transmission electron microscope (H-7650, Hitachi) without further staining. Myelin sheaths that were in contact with a DAB-positive OL process (external cytoplasmic tongue) were scored as mGFP-positive. Axon diameters and total fiber diameters (axon + myelin) of mGFP$^+$ and mGFP-negative internodes were measured from digital EM images (×15,000 magnification) using Image J (NIH) and EM-IP (Hitachi) software. Diameters were measured in two orthogonal directions avoiding the mesaxon (inner cytoplasmic loop) and averaged. The g-ratio was calculated as (axon diameter/ total fiber diameter).

Immunogold electron microscopy was carried out on ultracryosections of optic nerve as described previously (Akagi et al., 2006). Briefly, the fixed optic nerves were infused with 20% (w/v) polyvinylpyrrolidone, 1.8 M sucrose in 0.1 M phosphate buffer (pH 7) for 1 hr at 20°C–23°C, then overnight at 4°C. The infused specimens were frozen at −185°C in a rapid-freezing apparatus (KF-80, Leica) and ultrathin sections cut on an ultramicrotome (UCT or UC6, Leica) equipped with a cryoattachment (FCS or FC6, Leica). The sections were mounted on carbon-coated grids; after immunolabeling with anti-GFP (as above) for 24 hr at 4°C, they were incubated with colloidal gold (5 nm)-conjugated secondary anti-rabbit immunoglobulin G (1:100, Amersham) for 2 hr at 20°C–23°C.

SUPPLEMENTAL INFORMATION

Supplemental Information includes four figures and Supplemental Experimental Procedures and can be found with this article online at http://dx.doi.org/10.1016/j.neuron.2013.01.006.

REFERENCES

Akagi, T., Ishida, K., Hanasaka, T., Hayashi, S., Watanabe, M., Hashikawa, T., and Tohyama, K. (2006). Improved methods for ultracryotomy of CNS tissue

for ultrastructural and immunogold analyses. J. Neurosci. Methods *153*, 276–282.

Almeida, R.G., Czopka, T., Ffrench-Constant, C., and Lyons, D.A. (2011). Individual axons regulate the myelinating potential of single oligodendrocytes in vivo. Development *138*, 4443–4450.

Barres, B.A., Hart, I.K., Coles, H.S., Burne, J.F., Voyvodic, J.T., Richardson, W.D., and Raff, M.C. (1992). Cell death and control of cell survival in the oligodendrocyte lineage. Cell *70*, 31–46.

Barres, B.A., and Raff, M.C. (1993). Proliferation of oligodendrocyte precursor cells depends on electrical activity in axons. Nature *361*, 258–260.

Bartsch, S., Montag, D., Schachner, M., and Bartsch, U. (1997). Increased number of unmyelinated axons in optic nerves of adult mice deficient in the myelin-associated glycoprotein (MAG). Brain Res. *762*, 231–234.

Blakemore, W.F., and Murray, J.A. (1981). Quantitative examination of internodal length of remyelinated nerve fibres in the central nervous system. J. Neurol. Sci. *49*, 273–284.

Butt, A.M., Colquhoun, K., Tutton, M., and Berry, M. (1994). Three-dimensional morphology of astrocytes and oligodendrocytes in the intact mouse optic nerve. J. Neurocytol. *23*, 469–485.

Butt, A.M., Duncan, A., Hornby, M.F., Kirvell, S.L., Hunter, A., Levine, J.M., and Berry, M. (1999). Cells expressing the NG2 antigen contact nodes of Ranvier in adult CNS white matter. Glia *26*, 84–91.

Chehrehasa, F., Meedeniya, A.C., Dwyer, P., Abrahamsen, G., and Mackay-Sim, A. (2009). EdU, a new thymidine analogue for labelling proliferating cells in the nervous system. J. Neurosci. Methods *177*, 122–130.

Chong, S.Y.C., Rosenberg, S.S., Fancy, S.P.J., Zhao, C., Shen, Y.A., Hahn, A.T., McGee, A.W., Xu, X., Zheng, B., Zhang, L.I., et al. (2012). Neurite outgrowth inhibitor Nogo-A establishes spatial segregation and extent of oligodendrocyte myelination. Proc. Natl. Acad. Sci. USA *109*, 1299–1304.

Clarke, L.E., Young, K.M., Hamilton, N.B., Li, H., Richardson, W.D., and Attwell, D. (2012). Properties and fate of oligodendrocyte progenitor cells in the corpus callosum, motor cortex, and piriform cortex of the mouse. J. Neurosci. *32*, 8173–8185.

Dangata, Y.Y., Findlater, G.S., and Kaufman, M.H. (1996). Postnatal development of the optic nerve in (C57BL x CBA)F1 hybrid mice: general changes in morphometric parameters. J. Anat. *189*, 117–125.

Dangata, Y.Y., and Kaufman, M.H. (1997). Myelinogenesis in the optic nerve of (C57BL x CBA) F1 hybrid mice: a morphometric analysis. Eur. J. Morphol. *35*, 3–17.

Dimou, L., Simon, C., Kirchhoff, F., Takebayashi, H., and Götz, M. (2008). Progeny of Olig2-expressing progenitors in the gray and white matter of the adult mouse cerebral cortex. J. Neurosci. *28*, 10434–10442.

Einheber, S., Zanazzi, G., Ching, W., Scherer, S., Milner, T.A., Peles, E., and Salzer, J.L. (1997). The axonal membrane protein Caspr, a homologue of neurexin IV, is a component of the septate-like paranodal junctions that assemble during myelination. J. Cell Biol. *139*, 1495–1506.

Fields, R.D. (2008). White matter in learning, cognition and psychiatric disorders. Trends Neurosci. *31*, 361–370.

Foster, R.E., Connors, B.W., and Waxman, S.G. (1982). Rat optic nerve: electrophysiological, pharmacological and anatomical studies during development. Brain Res. *255*, 371–386.

Fruttiger, M., Calver, A.R., and Richardson, W.D. (2000). Platelet-derived growth factor is constitutively secreted from neuronal cell bodies but not from axons. Curr. Biol. *10*, 1283–1286.

Guo, F., Maeda, Y., Ma, J., Xu, J., Horiuchi, M., Miers, L., Vaccarino, F., and Pleasure, D. (2010). Pyramidal neurons are generated from oligodendroglial progenitor cells in adult piriform cortex. J. Neurosci. *30*, 12036–12049.

Hippmeyer, S., Vrieseling, E., Sigrist, M., Portmann, T., Laengle, C., Ladle, D.R., and Arber, S. (2005). A developmental switch in the response of DRG neurons to ETS transcription factor signaling. PLoS Biol. *3*, e159. http://dx.doi.org/10.1371/journal.pbio.0030159.

Honjin, R., Sakato, S., and Yamashita, T. (1977). Electron microscopy of the mouse optic nerve: a quantitative study of the total optic nerve fibers. Arch. Histol. Jpn. *40*, 321–332.

Kang, S.H., Fukaya, M., Yang, J.K., Rothstein, J.D., and Bergles, D.E. (2010). NG2⁺ CNS glial progenitors remain committed to the oligodendrocyte lineage in postnatal life and following neurodegeneration. Neuron *68*, 668–681.

Kimura, F., and Itami, C. (2009). Myelination and isochronicity in neural networks. Front. Neuroanat. *3*, 12. http://dx.doi.org/10.3389/neuro.05.012. 2009.

Lasiene, J., Shupe, L., Perlmutter, S., and Horner, P.J. (2008). No evidence for chronic demyelination in spared axons after spinal cord injury in a mouse. J. Neurosci. *28*, 3887–3896.

Lasiene, J., Matsui, A., Sawa, Y., Wong, F., and Horner, P.J. (2009). Age-related myelin dynamics revealed by increased oligodendrogenesis and short internodes. Aging Cell *8*, 201–213.

Makinodan, M., Rosen, K.M., Ito, S., and Corfas, G. (2012). A critical period for social experience-dependent oligodendrocyte maturation and myelination. Science *337*, 1357–1360.

McCarthy, G.F., and Leblond, C.P. (1988). Radioautographic evidence for slow astrocyte turnover and modest oligodendrocyte production in the corpus callosum of adult mice infused with 3H-thymidine. J. Comp. Neurol. *271*, 589–603.

McIver, S.R., Lee, C.S., Lee, J.M., Green, S.H., Sands, M.S., Snider, B.J., and Goldberg, M.P. (2005). Lentiviral transduction of murine oligodendrocytes in vivo. J. Neurosci. Res. *82*, 397–403.

Murtie, J.C., Macklin, W.B., and Corfas, G. (2007). Morphometric analysis of oligodendrocytes in the adult mouse frontal cortex. J. Neurosci. Res. *85*, 2080–2086.

Peters, A. (2009). The effects of normal aging on myelinated nerve fibers in monkey central nervous system. Front. Neuroanat. *3*, 11. http://dx.doi.org/10.3389/neuro.05.011.2009.

Peters, A., and Kemper, T. (2012). A review of the structural alterations in the cerebral hemispheres of the aging rhesus monkey. Neurobiol. Aging *33*, 2357–2372.

Power, J., Mayer-Pröschel, M., Smith, J., and Noble, M. (2002). Oligodendrocyte precursor cells from different brain regions express divergent properties consistent with the differing time courses of myelination in these regions. Dev. Biol. *245*, 362–375.

Pringle, N., Mudhar, H., Collarini, E.J., and Richardson, W.D. (1992). PDGF receptors in the CNS: during late neurogenesis, expression of PDGF alpha receptor appears to be restricted to glial cells of the oligodendrocyte lineage. Development *115*, 535–552.

Psachoulia, K., Jamen, F., Young, K.M., and Richardson, W.D. (2009). Cell cycle dynamics of NG2 cells in the postnatal and ageing brain. Neuron Glia Biol. *5*, 57–67.

Raz, N., Dotan, S., Chokron, S., Ben-Hur, T., and Levin, N. (2012). Demyelination affects temporal aspects of perception: an optic neuritis study. Ann. Neurol. *71*, 531–538.

Richardson, W.D., Young, K.M., Tripathi, R.B., and McKenzie, I. (2011). NG2-glia as multipotent neural stem cells: fact or fantasy? Neuron *70*, 661–673.

Richter-Landsberg, C., and Gorath, M. (1999). Developmental regulation of alternatively spliced isoforms of mRNA encoding MAP2 and tau in rat brain oligodendrocytes during culture maturation. J. Neurosci. Res. *56*, 259–270.

Rivers, L.E., Young, K.M., Rizzi, M., Jamen, F., Psachoulia, K., Wade, A., Kessaris, N., and Richardson, W.D. (2008). PDGFRA/NG2 glia generate myelinating oligodendrocytes and piriform projection neurons in adult mice. Nat. Neurosci. *11*, 1392–1401.

Sandell, J.H., and Peters, A. (2002). Effects of age on the glial cells in the rhesus monkey optic nerve. J. Comp. Neurol. *445*, 13–28.

Skoff, R.P., Price, D.L., and Stocks, A. (1969). Electron microscope autoradiographic studies of gliogenesis in rat optic nerve II. Time of origin. J. Comp. Neurol. *169*, 313–334.

Simon, C., Götz, M., and Dimou, L. (2011). Progenitors in the adult cerebral cortex: cell cycle properties and regulation by physiological stimuli and injury. Glia 59, 869–881.

Srinivas, S., Watanabe, T., Lin, C.S., William, C.M., Tanabe, Y., Jessell, T.M., and Costantini, F. (2001). Cre reporter strains produced by targeted insertion of EYFP and ECFP into the ROSA26 locus. BMC Dev. Biol. 1, 4.

Stallcup, W.B., and Beasley, L. (1987). Bipotential glial precursor cells of the optic nerve express the NG2 proteoglycan. J. Neurosci 7, 2737–2744.

Stanford, L.R. (1987). Conduction velocity variations minimize conduction time differences among retinal ganglion cell axons. Science 238, 358–360.

Stidworthy, M.F., Genoud, S., Süter, U., Mantei, N., and Franklin, R.J. (2003). Quantifying the early stages of remyelination following cuprizone-induced demyelination. Brain Pathol. 13, 329–339.

Sturrock, R.R. (1980). Myelination of the mouse corpus callosum. Neuropathol. Appl. Neurobiol. 6, 415–420.

Trapp, B.D., Nishiyama, A., Cheng, D., and Macklin, W. (1997). Differentiation and death of premyelinating oligodendrocytes in developing rodent brain. J. Cell Biol. 137, 459–468.

Tripathi, R.B., Rivers, L.E., Young, K.M., Jamen, F., and Richardson, W.D. (2010). NG2 glia generate new oligodendrocytes but few astrocytes in a murine experimental autoimmune encephalomyelitis model of demyelinating disease. J. Neurosci. 30, 16383–16390.

Vinet, J., Lemieux, P., Tamburri, A., Tiesinga, P., Scafidi, J., Gallo, V., and Sík, A. (2010). Subclasses of oligodendrocytes populate the mouse hippocampus. Eur. J. Neurosci. 31, 425–438.

Wake, H., Lee, P.R., and Fields, R.D. (2011). Control of local protein synthesis and initial events in myelination by action potentials. Science 333, 1647–1651.

Young, K.M., Merson, T.D., Sotthibundhu, A., Coulson, E.J., and Bartlett, P.F. (2007). p75 neurotrophin receptor expression defines a population of BDNF-responsive neurogenic precursor cells. J. Neurosci. 27, 5146–5155.

Zhu, X., Hill, R.A., Dietrich, D., Komitova, M., Suzuki, R., and Nishiyama, A. (2011). Age-dependent fate and lineage restriction of single NG2 cells. Development 138, 745–753.

Zatorre, R.J., Fields, R.D., and Johansen-Berg, H. (2012). Plasticity in gray and white: neuroimaging changes in brain structure during learning. Nat. Neurosci. 15, 528–536.

Zawadzka, M., Rivers, L.E., Fancy, S.P.J., Zhao, C., Tripathi, R., Jamen, F., Young, K., Goncharevich, A., Pohl, H., Rizzi, M., et al. (2010). CNS-resident glial progenitor/stem cells produce Schwann cells as well as oligodendrocytes during repair of CNS demyelination. Cell Stem Cell 6, 578–590.